表2　国立循環器病研究センターにおける心臓移植(2)

待機状況	Status 1：39［LVAS：34（87%）］
LVAS	Nipro（Toyobo）：29, HeartMate VE：2
	Novacor：1，EVAHEART：1，Jarvik 2000：1
待機期間	29～2,751（mean：982）日
	［Status 1：29～1,476（mean：818）日］
LVAS 補助期間	39～1,730（平均：882）日
結果	退院：37
	外来：36，死亡：1（4年2月感染）
	入院加療中：2

表3　同時心臓移植施行例における時間経過

事項	症例1	症例2
LVAS 装着	植込型：HMVE	体外設置型：Nipro
補助期間	993日	838日
ドナー情報	06:58	06:58
ドナーチーム出発	10:15	10:16
ドナー評価	14:36	16:52
レシピエント手術開始	14:40	17:40
ドナー心大動脈遮断	16:27	18:03
ドナー心到着	17:24	20:44
レシピエント大動脈遮断解除	18:44	21:52
ICU から移植病棟へ	第5病日	第5病日
退院	第50病日	第50病日

ナルドナー（7例）において，術後管理および経過での有意な差は認めず，36例全例が生存退院した。

移植手術は，第1例目をLower-Shumway法，第2例目をbi-caval法にて施行したが，第3例目以降はmodified bi-caval法にて行っている[3]。また，心筋保護液は，当初St.Thomas液を用いたが，7例目からはCelsior液を用いている。免疫抑制療法は，カリシニューリンインヒビター［cyclosporin（CyA）あるいはtacrolimus（Tac）］，mycophenolate mofetil（MMF）およびステロイドによる3者併用を行っている[3]。カリシニューリンインヒビターは，当初はCyAを用いたが，その後CyAあるいはTacを用いるようになり，最近ではTacを第一選択としている。Induction therapyは，腎機能障害例等で行ってきた。当初はOKT3を，最近ではbasiliximab（シムレクト）を使用している[3]。

抗体関連型拒絶反応に対しては，PRA検査等を実施し，病理所見とあわせて必要に応じて，ガンマグロブリン投与や血漿交換を行っている[3]。

心臓移植後の生存率を図3に示すが，1例が4年2カ月後に感染症で死亡したが，移植後早期の2例以外は外来加療中であり，12年以上経過するものが2例である。移植後12年における生存率は95.2%と国際心肺移植学会レジストリーより良好な成績を示している[3]。

改正臓器移植法施行に伴い，18歳未満からの臓器提供が可能となった。心臓移植においては，18歳未

表4　国立循環器病研究センターにおけるマージナルドナー criteria と症例

下記いずれかでマージナルドナーと判定された症例	29例
1. 年齢：50歳以上	8例
2. サイズミスマッチ（ドナー/レシピエント体重比：0.8以下）	4例
3. 4時間以上の虚血	1例
4. 心肥大（壁厚＞13 mm，ECG上明らかなLVH）	2例
5. 最近の心肺蘇生の既往	14例
6. 高容量の強心薬（DOA 10 γまたはアドレナリン0.06 γ以上）	13例
7. LVEF：45%以下	0例
	（45–55%は6例）

表5　国立循環器病研究センターにおける術後管理と経過

Variables（治療と経過）	マージナルドナー	非マージナル	p
術後DOA/DOB最大使用量（γ）	7.1±3.2	5.1±2.7	0.1356
DOA/DOB投与期間（日）	6.2±5.0	4.9±3.5	0.5391
Epinephrine使用例	4	0	0.2973
IABP使用例	2（1例はPCPSと併用）	0	0.4746
PCPS使用例	1	0	0.6255
挿管日数（日）	1.1±1.1	0.7±0.6	0.3671
ICU滞在日数（日）	6.2±3.3	7.9±6.4	0.3531
Primary Graft Failure（PGF）	2	0	0.4746

満からの提供に対しては，登録時の年齢が18歳未満の症例を優先することとなり，患者選択における医学的緊急度や血液型への対応は同様となった。当センターにおいても，本年9月に18歳未満からの臓器提供に基づく心臓移植を10歳代の男児に施行した。この患者はLVASによる補助を764日行い，Status 1にて341日間待機中であった。わが国での平均Status 1待機期間が841日に比して，短期間で心臓移植が実施された。

わが国における心臓移植の動向

わが国においては，2011年9月10日までに110例の心臓移植が実施されたが，全例Status 1で89%がLVASによるブリッジ例であり，待機期間は，平均841日であった。これまでに5例が死亡したが，10年生存率は80.0%であった。2011年8月31日における日本臓器移植ネットワークへの累積登録患者数は521名で，わが国で108例（心肺を除く）の心臓移植が実施されたが，待機中の患者190名あり，そのうち120例はStatus 1での待機である（**図4**）。心臓移植施行数は増加したものの，待機者数も増加傾向にある（**表6**）。このため，待機日数は減少していない。当センターにおいても，**図5**で示すように，改正前に施行した27例と改正後の12例で待機日数（Status 1）および補助期間をみると，現状では，改正後の実施例に

図3　NCVCにおける心臓移植の成績

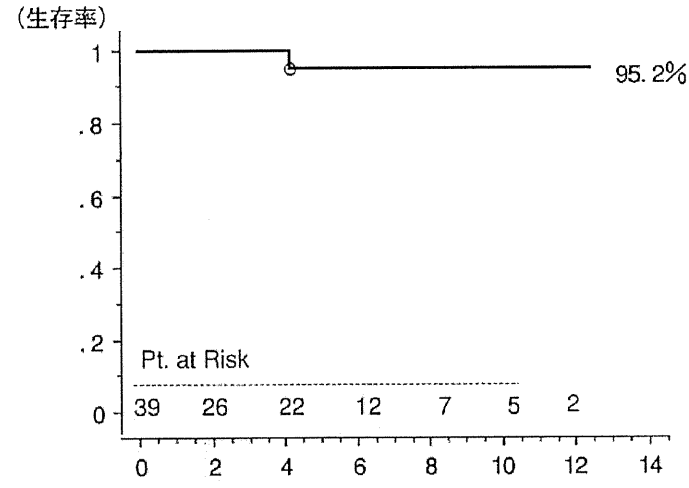

図4　わが国における医学的緊急度による心臓移植希望登録者数

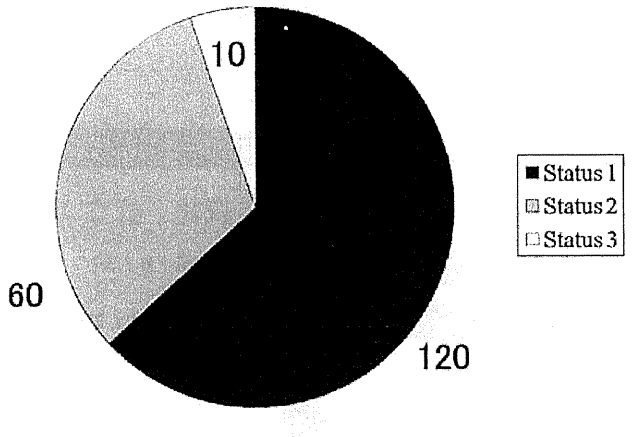

(Japan Organ Transplant Network)
(n=190，2011.8.31 現在)

表6　日本臓器移植ネットワークへの累積登録者数（心臓移植）

現登録者数	190
既登録者	331*
死体移植済	109*
海外渡航	41
取消	17
死亡	164
登録者累計	521

(2011年8月31日現在)
：4例心肺移植，：1例心肺移植

おいて著明に増加していた。

わが国における臓器提供においては，メディカルコンサルタント制度をとるようになり，提供臓器数が多く，また，その生着率も高い（図6）。しかし，心臓移植希望者数も多いため，今後も長期の心臓移植待機を要するものと考えられる。

このため，今後さらにLVASによる心臓移植へのブリッジ例が増加し，さらにその補助期間も長期に及ぶと想定される。このようなLVASによる長期の補助を行う症例への対応として，装着患者のQOL向上が期待できる植込型補助人工心臓の早期導入が望まれてきた。国産のEVAHEARTおよびDuraHearを含む在宅管理ができる植込型LVASの臨床応用を進めるため

図 5　NCVC における心臓移植実施状況

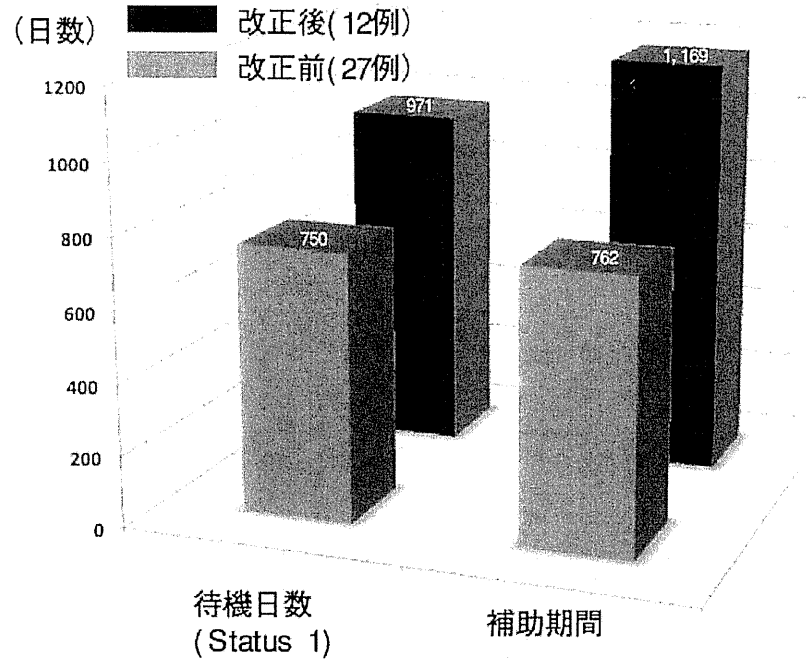

図 6　脳死下臓器移植と生着状況（1997.10～2010.12）

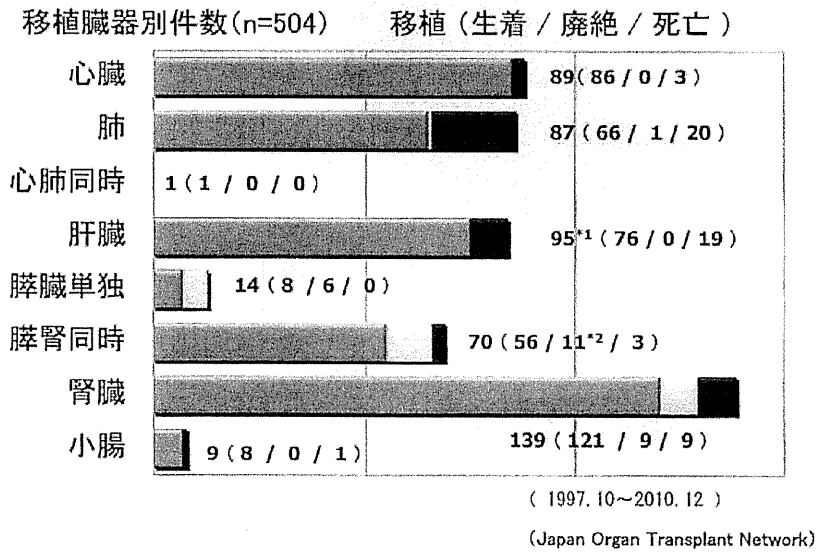

*1：分割肝移植 6 提供 12 移植を含む
*2：膵もしくは腎のみ廃絶

に，補助人工心臓関連学会協議会を含めた関係者により作業が進められた結果，2010 年 12 月に国産 2 種が製造販売承認され，本年 3 月には保険収載された（図 7）。さらに，現在 2 機種の審査が進められている。また，このような多機種の植込型補助人工心臓を同じプロトコールで実施する市販後のデータ収集を行うために，医薬品医療機器総合機構，関連学会，医療機関，補助人工心臓関連企業による Japanese registry for Mechanically Assisted Circulatory Support（J-MACS）が設立された。当初は，植込型 LVAS に順じた適応を行う

図7　わが国におけるVASの治験/製造販売承認/健康保険収載

	治験	承認	収載
体外設置拍動流型			
Nipro(Toyobo)	1986	1990	1994
Zeon	1986	1990	1994*
植込拍動流型			
Novacor	1996	2001	2004★
HeartMate XVE	2001	2009	?
植込無拍動流型			
EVAHEART	2005	2010	2011(3月)
Jarvik 2000	2008	?	?
DuraHeart	2008	2010	2011(3月)
Heartmate II	2010	?	?

*：2005年撤退、★：2006.年撤退

図8　J-MACSへの補助人工心臓登録数の推移

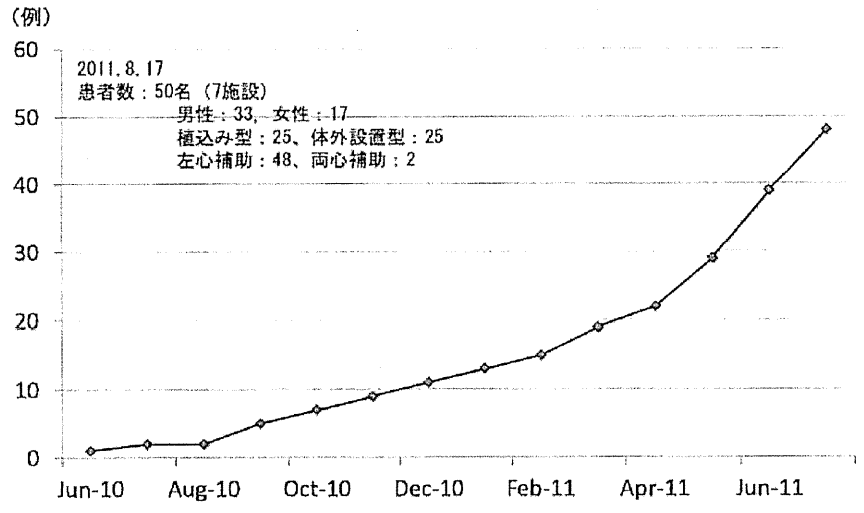

J-MACS:Japanese registry for Mechanically Assisted Circulatory Support

PMDA ホームページより;http://www.info.pmda.go.jp/kyoten_kiki/track.html

Nipro(Toyobo)LVASにおいてデータ収集を開始した。2種の植込型LVASが保険償還されてからは，植込型LVASの症例登録が増加している（図8）。J-MACSにより植込型LVASの適応決定や管理法の改善が図られることにより，心臓移植待機中にLVASによるブリッジを必要とする患者における成績向上が期待されている。

おわりに

当センターではこれまで39例の心臓移植を実施してきた。従来，施行数は年に数例であったが，改正臓器移植法実施後は，施行数の増加とともに，毎週施行することもみられるようになった。しかし，待機期間は長期に及んだままであり，多くは，LVAS装着例であった。長期待機においては，経過中の感染管理，栄

養管理を含む患者の全身状態維持が重要である。また，LVAS装着例では，心臓移植によりLVASを除去してから本格的なリハビリを行える症例も多い。このため，当センターでは，医師，看護師のみならず，レシピエント移植コーディネーター，人工心臓管理技術認定士，メディカルソーシャルワーカー，薬剤師，理学療法士，臨床工学技士，栄養士，栄養サポートチーム，感染制御チーム，精神科などのチームで治療を進めている。また，ドナー情報発生時には，ドナーチームの派遣を迅速に行うとともに，短い虚血許容時間に対するレシピエント手術への対応として，夜間や休日での施行も多くなるため，手術室，ICUのみならず，輸血管理室や臨床検査部門，事務部門と連携して対応してきた。このように，レシピエント候補はLVAS装着による長期待機例が大部分をしめるなかで，ドナー心の状況に応じた対応を行いながら心臓移植を実施してきた。

今後，心臓移植数の増加のみならず，待機患者数の増加も見込まれており，心臓移植施設として院内体制の整備をさらに進めることが重要である。また，小児心臓移植への対応も今後の課題である。

文　献

1) 日本心臓移植研究会. 本邦心臓移植登録報告(2010年). 移植 2010; 45: 633-637.
2) Kitamura S, Nakatani T, Bando K, *et al.* Modification of bicaval anastomosis technique for orthotopic heart transplantation. Ann Thorac Surg 2001; 72: 1405-1406.
3) Nakatani T. Heart transplantation. Circ J 2009; 73 Suppl A: A55-A60.
4) Wada K, Takada M, Kotake T, *et al.* Limited sampling strategy for mycophenolic acid in Japanese heart transplant recipients: comparison of cyclosporin and tacrolimus treatment. Circ J 2007; 71: 1022-1028.
5) 簗瀬正伸，中谷武嗣. 心臓移植抗体関連拒絶反応の診断と治療. 心臓 2010; 42: 20-25.
6) Stehlik J, Edwards LB, Kucheryavaya AY, *et al.* The Registry of the International Society for Heart and Lung Transplantation: Twenty-eighth Adult Heart Transplantation Report-2011. J Heart Lung Transplant 2011; 30: 1078-1094.

REVIEW / SYNTHÈSE

Roles of guanylyl cyclase-A signaling in the cardiovascular system

Yoshihiko Saito, Ichiro Kishimoto, and Kazuwa Nakao

Abstract: Atrial natriuretic peptide (ANP) and B-type natriuretic peptide (BNP) are cardiac hormones synthesized in and secreted from the heart. ANP and BNP bind the common receptor guanylyl cyclase-A (GC-A) and possess biological actions. Based on their diuretic, natriuretic, and vasodilating activities, they are now widely used as therapeutic agents for heart failure. Roles of endogenous ANP and BNP have been investigated using mice lacking the gene encoding GC-A. Here we describe the recent understanding of roles of GC-A in the cardiovascular system.

Résumé : Le peptide natriurétique auriculaire (PNA) et le peptide natriurétique de type B (PNB) sont des hormones cardiaques synthétisées dans le cœur et sécrétées par celui-ci. Le PNA et le PNB se lient au récepteur de la guanylyl cyclase A (GC-A) et exercent des actions biologiques. Ils sont largement utilisés comme agents thérapeutiques pour traiter l'insuffisance cardiaque en raison de leurs activités diurétiques, natriurétiques et vasodilatatrices. Les rôles du PNA et du PNB endogènes ont été examinés chez des souris déficientes pour le gène codant pour la GC-A. Dans le présent article, nous décrivons les récentes avancées dans la compréhension des rôles de la GC-A dans le système cardiovasculaire.

[Traduit par la Rédaction]

Introduction

Atrial natiuretic peptide (ANP) and B-type natriuretic peptide (BNP), cardiac hormones that are mainly synthesized in and secreted from the heart, bind the common receptor guanylyl cyclase-A (GC-A) and lead their biological activities, diureis, natriuresis, and vasodilation. In addition to these pharmacological activities, genetically engineered mice lacking the gene encoding the GC-A gene show the roles of endogenous ANP and BNP.

The first report of GC-A knockout (KO) mice, generated in 1995 by Lopez et al. (1995), showed salt-resistant hypertension with marked left ventricular hypertrophy in GC-A KO mice, suggesting a cardioprotective effect of GC-A signaling. Using GC-A conventional and conditional KO mice, several investigators have reported the roles of the endogenous GC-A signaling pathway in pathological settings. The manuscript focuses the recent understanding of roles of the GC-A signaling by us and others.

Roles of GC-A signaling in hypertension

As mentioned above, GC-A KO mice showed salt-resistant hypertension (Lopez et al. 1995), but ANP KO mice showed salt-sensitive hypertension (John et al. 1995). The precise reason for the difference in salt dependency between ligand and receptor KO mice is still unclear. Acute administration of ANP decreased blood pressure via a nonendothelial cell (EC)-dependent manner. Vascular ECs expressed GC-A, although they predominantly express guanylyl cyclase-B (GC-B), whose natural ligand is C-type natriuretic peptide (Nakao et al. 1992). Of course, GC-A is expressed in vascular smooth muscle cells (SMCs) and cardiomyocytes (Nakao et al. 1992). The mechanism for hypertension in GC-A KO mice has been intensively investigated by Kuhn's laboratory (Holtwick et al. 2002, 2003; Sabrane et al. 2005, 2009) using SMC- (Holtwick et al. 2002) or EC- (Sabrane et al. 2005, 2009) specific GC-A KO mice (Table 1).

SMC-specific GC-A KO (SMC-GC-A KO) mice exhibit blood pressure equal to that of control mice (GC-$A^{flox/flox}$), but have no hypotensive response to exogenously administered ANP (Holtwick et al. 2002). In EC-specific GC-A KO (EC-GC-A KO) (Sabrane et al. 2005), blood pressure is similarly elevated to the level in conventional GC-A KO mice, and exogenous ANP injection significantly decreases blood pressure. Sabrane et al. (2009) also proved that ANP enhances microvascular endothelial macromolecule permeability in

Received 5 January 2011. Accepted 19 March 2011. Published at www.nrcresearchpress.com/cjpp on 14 June 2011.

Y. Saito. First Department of Internal Medicine, Nara Medical University, Kashihara, Nara 634-8522, Japan.
I. Kishimoto. National Cardiovascular Research Center, Suita, Japan.
K. Nakao. Department of Clinical Science and Medicine, Kyoto Graduate School of Medicine, Kyoto, Japan.

Corresponding author: Yoshihiko Saito (e-mail: yssaito@naramed-u.ac.jp).

This paper is one of a selection of papers published in the Special Issue entitled The endocrine heart, 30 years later: 23rd International Society of Hypertension Meeting, and has undergone the Journal's usual peer-review process.

Table 1. Blood pressure in tissue-specific GC-A KO mice.

	BP	BP response to ANP	Permeability response to ANP
Floxed GC-A	→	↓	Yes
Straight GC-A KO	↑	→	No
SMC-GC-A KO	→	→	Not done
EC-GC-A KO	↑	↓	No

Note: GC-A, guanylyl cyclase-A; KO, knockout; BP, blood pressue; ANP, atrial natriuretic peptide; SMC; smooth muscle cell; EC, endothelial cell.

Fig. 1. Targeted deletion of angiotensin II type I receptor a (AT1a) ameliorated hypertension, cardiac hypertrophy, and interstitial fibrosisin guanylyl cyclase-A (GC-A) knockout (KO) mice: (A) systolic blood pressure (SBP); (B) heart weight / body weight (HW/BW); (C) left ventricular weight / body weight (LVW/BW); (D) representative examples of fibrosis visualized with van Gieson stain (red); magnification 200×; (E) left ventricular interstitial fibrosis. Values are means with bars indicating SE (n = 12–16). *, $P < 0.05$. (From Li et al. 2002, reproduced with permission of Circulation, Vol. 106, p. 1724, © 2002 American Heart Association.)

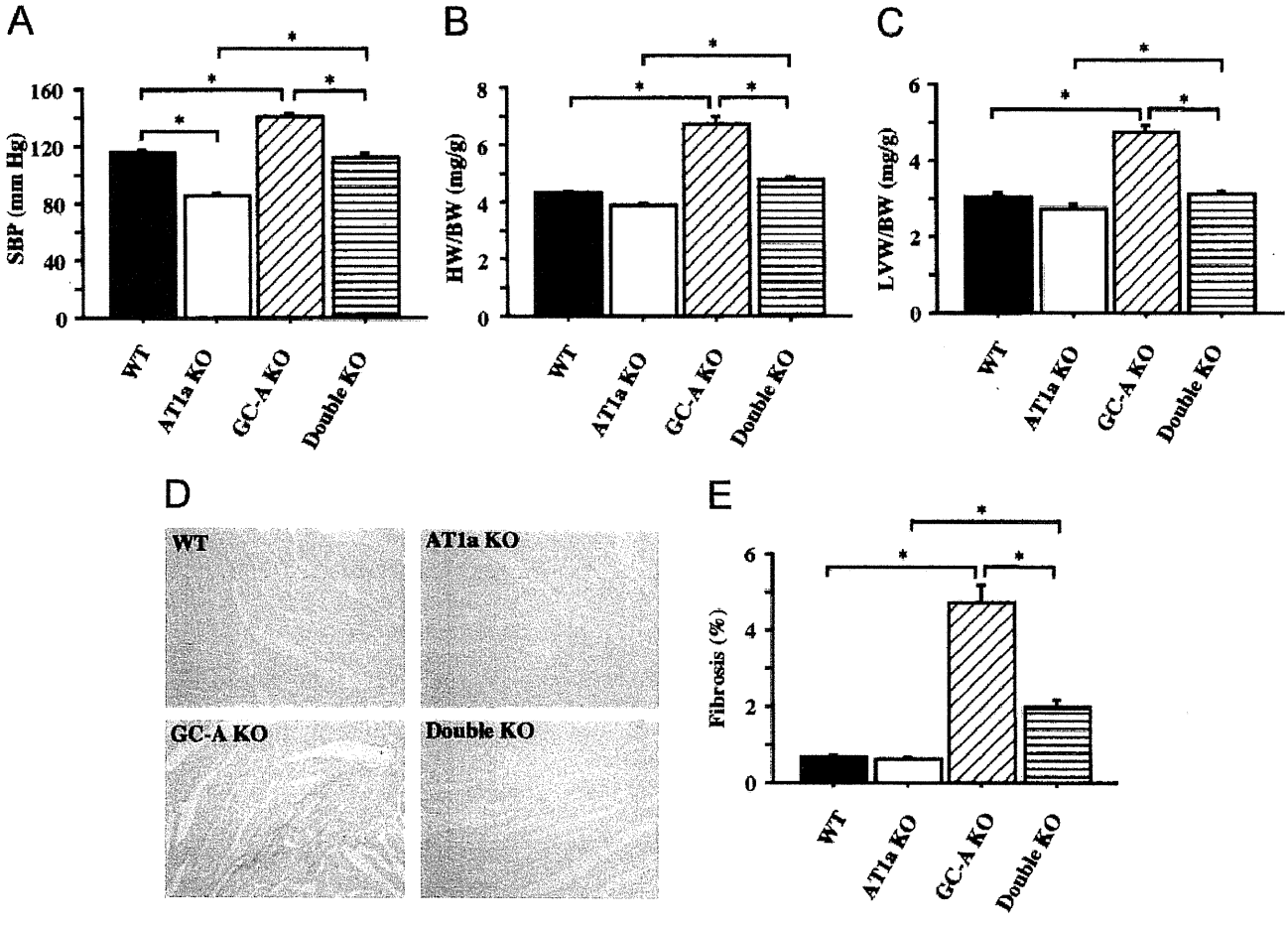

vivo. These results clearly indicate that hypertension in GC-A KO is endothelium dependent but not SMC dependent. In contrast, the acute depressor effect of exogenously administered ANP is endothelium independent but SMC dependent. It remains unknown which channels or transporters are involved in GC-A-mediated permeation in ECs.

Roles of GC-A signaling in cardiac remodeling

GC-A KO mice show salt-insensitive hypertension associated with left ventricular hypertrophy and fibrosis. To circumvent the effect of hypertension on cardiac remodeling, Holwick et al. generated the cardiomyocyte-specific GC-A KO (CM-GC-A KO) mice (Holtwick et al. 2003). In CM-GC-A KO mice, systemic blood pressure is significantly lower than that in control mice (GC-$A^{flox/flox}$), probably because of the elevated systemic levels and endocrine actions of ANP. CM-GC-A KO mice showed a significantly larger ratio of heart weight to body weight accompanied with higher expression levels of hypertrophy marker genes, ANP, α-skeletal actin, and β-myosin heavy chain, clearly demon-

Fig. 2. Guanylyl cyclase-A (GC-A) disruption-induced gender-related differences in cardiac hypertrophy and fibrosis were inhibited by castration in male (Cast), but not in female (OVX) mice that were castrated at 10 weeks and analyzed at 16 week of age. The ratio of the areas of van Gieson-stained interstitial fibrosis to the total left ventricular area was calculated using image analysis software and a Zeiss KS400 system. (A) LVW/BW ratio; (B) relative levels of left ventricular fibrosis; (C) photomicrographs showing representative examples of cardiac fibrosis (red) (magnification, 200×). Values are means ± SE; n = 7–9 per group. *, $P < 0.05$. (From Li et al. 2004, reproduced with permission of Endocrinology, Vol. 145, p. 953, © 2004 The Endocrine Society.)

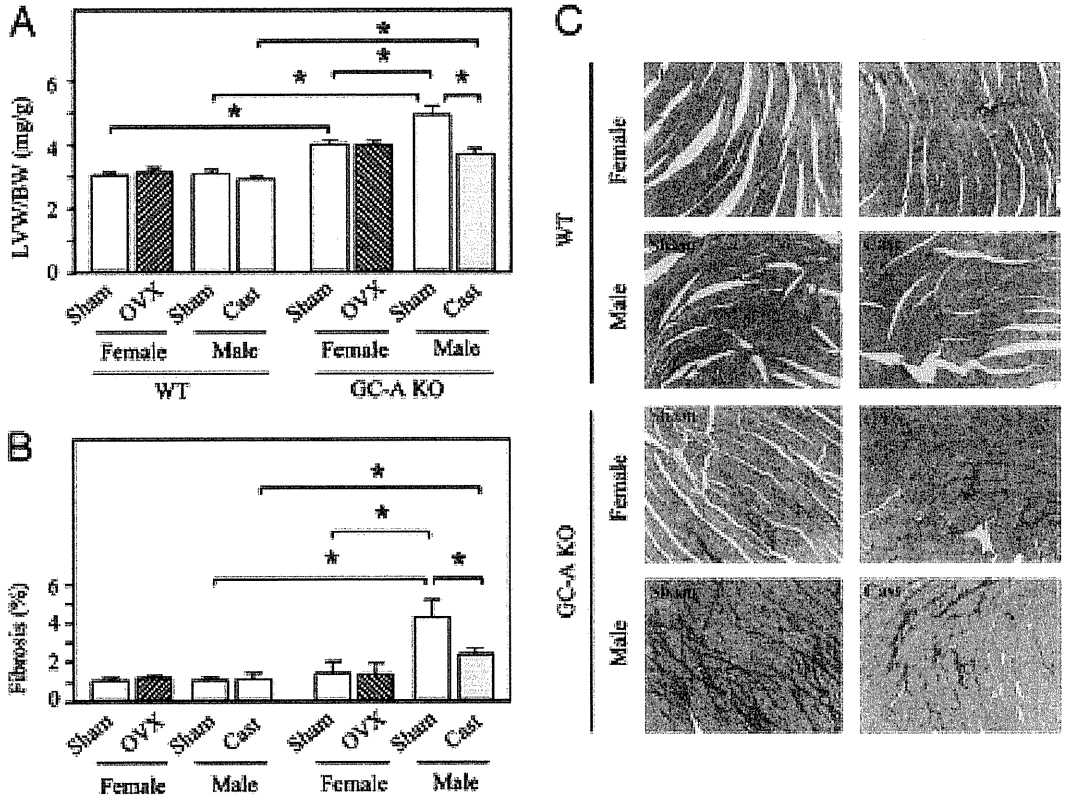

strating that GC-A signaling is involved in molecular program of cardiac hypertrophy. Interestingly, in contrast to the hypertrophic phenotype, the size of the fibrotic area was similar in both CM-GC-A KO and wild-type mice. Although the mechanism is still unclear, there would be 2 possible mechanisms, one being that fibrosis is closely related to the elevation of blood pressure and another that nonmyocytes are involved. Given that left ventricular fibrosis is augmented in BNP KO mice, in which systemic blood pressure is equal to that of wild-type mice (Tamura et al. 2000), contribution of nonmyocytes to the generation of fibrosis is important.

GC-A signaling inhibits AT1 signaling

Given the evidence that the actions of ANP and BNP are functionally opposite to those of angiotensin II and aldosterone, and that ANP attenuates angiotensin II-induced vasocontraction and inhibits aldosterone secretion, we hypothesized that GC-A signaling is counteracting angiotensin II- or aldosterone-induced cardiac remodling. To assess the scenario, we crossed the GC-A KO mice with mice lacking the gene encoding the type 1 angiotensin II (AT1) receptor (Li et al. 2002). Systolic blood pressure is similarly reduced by about 20% because of genetic blockade of the AT1 signaling in both GC-A KO mice and wild-type mice (Fig. 1*a*). Thus, hypertension in GC-A KO mice is not AT1 dependent. However, genetic blockage of the AT1 gene significantly and almost completely decreased the ratio of left ventricular weight to body weight and fibrotic area in GC-A KO mice but it did not affect the ratio in wild-type mice, indicating that cardiac remodeling in GC-A KO mice is AT1 dependent (Fig. 1)

Next we investigated whether pharmacological blockade of AT1 signaling by the AT1 receptor blocker olmésartan improves cardiac remodeling after its establishment (Li et al. 2002). Olmesartan at a dose of 10 $mg \cdot kg^{-1} \cdot day^{-1}$ was given orally by gavage for 4 weeks from 12 weeks of age, because hypertension and ventricular remodeling were accomplished at the age of 12 weeks old. Olmesartan treatment significantly decreased systolic blood pressure by about 20% in both genotypes of mice and reduced hypertrophy and fibrosis. These decrements were similar to those observed by genetic blockage of AT1. To rule out the possibility that genetic and pharmacological blockade of AT1 signaling on cardiac remodeling resulted from a change in systolic blood pressure, we investigated the blood pressure lowering effect of hydralagine on cardiac hypertrophy and fibrosis in GC-A KO mice. Hydralagine at a dose of 24 $mg \cdot kg^{-1} \cdot day^{-1}$ lowered blood pressure but enhanced left ventricular hypertrophy via GC-A

Fig. 3. Survival curve and ventricular remodeling after permanent coronary ligation in guanylyl cyclase-A (GC-A) knockout (KO) mice and double-KO mice lacking both GC-A and type 1 angiotensin receptor genes. (A) Kaplan–Meier survival curve in GC-A KO mice, GC-A KO mice with hydralazine treatment, and double KO mice after permanent coronary ligation. (B) Collagen volume fraction (%) in the ventricles 4 weeks after coronary ligation (right) and sham-operated mice (left). Values are means ± SE. *, $P < 0.05$ vs. wild type; †, $P < 0.05$ vs. sham-operated mice; ‡, $P < 0.001$ vs. GC-A KO. (C) Representative histological examination with von Gieson staining in 4 genotypes of mice. WT, wild type; MI, myocardial infarction; DKO; double-KO mice; h-KO, GC-A KO mice with hydralazine treatment). (Adapted from Nakanishi et al. 2005, reproduced with permission of Hypertension, Vol. 46, p. 445, © 2005 American Heart Association.)

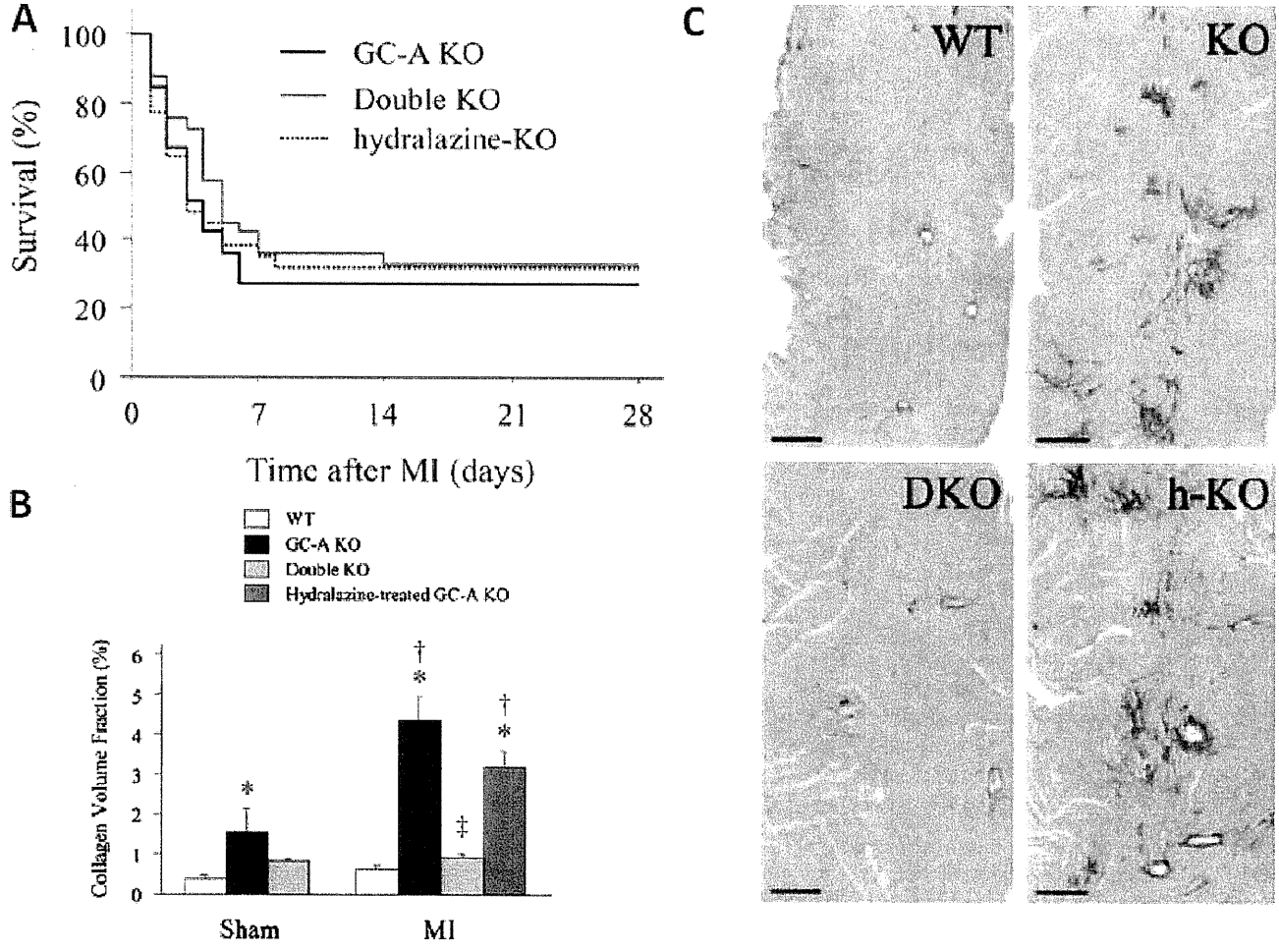

and the type 2 angiotensin receptor pathway, although it partially inhibited fibrosis in GC-A KO mice via GC-A and the AT1 pathway (Li et al. 2010). These findings indicate that GC-A signaling functionally antagonized AT1 signaling in cardiac remodeling in a blood pressure independent manner. This was also confirmed by the evidence that a subpressor dose of angiotensin II administration exaggerated hypertrophy and fibrosis without blood pressure change (Li et al. 2002). Interestingly, cardiac phenotypes in male GC-A KO mice were significantly more severe than those in female GC-A KO mice (Fig. 2) (Li et al. 2004). Although ovariectomy did not influence fibrotic area in female GC-A KO mice, castration reduced fibrotic area in male GC-A KO mice. The mechanism for the gender difference is the slightly higher expression level of angiotensinogen in the male heart. Angiotensinogen mRNA was similarly higher in the heart of both male wild-type and GC-A KO mice than in that of both female wild-type and GC-A KO mice. However, wild-type mice showed no gender difference in cardiac hypertrophy or fibrosis, probably because GC-A signaling inhibited the relatively activated renin–angiotensin system in the male heart.

The mechanism of the inhibitory effect of GC-A signaling on AT1 signaling was elucidated by Kishimoto's laboratory. In GC-A KO mice, the AT1 mRNA level did not change compared with that in wild-type mice. So GC-A signaling inhibits AT1 signaling mainly via the intracellular mechanism. cGKI binds directly to and phosphorylates–activates RGS2, which terminates G_q-coupled receptor signaling in vascular smooth muscle (Tang et al. 2003). Consistent with this, Tokudome et al. reported that cardiomyocyte-specific overexpression of RGS4, the major RGS protein in cardiomyocytes, significantly reduced hypertrophy, cardiomyocyte size, and ventricular calcineurin activity in GC-A-KO mice (Tokudome et al. 2008). Thus, the possible mechanism of the antagonistic action of GC-A signaling against AT1 signaling may be explained by GC-A–cGKI–RGS4 interaction.

GC-A signaling functionally inhibits signaling pathways driven by mineralocorticoid receptor

Next we investigated the effect of the aldosterone blocker eplerenone on cardiac hypertrophy and fibrosis in GC-A KO mice. Treatment with eplerenone at a dose of 50 $mg \cdot kg^{-1} \cdot day^{-1}$ lowered systolic blood pressure by about 20 mm Hg and reduced significantly the heart weight / body weight ratio and fibrotic area, accompanied with a reduction in expression levels of ANP, BNP, collagen type I, and collagen type IV genes (Zhang et al. 2008). Taking into account the inhibitory effect of ANP in aldosterone synthesis from cultured adrenal cells, aldosterone production would be elevated in the heart of GC-A KO mice. However, the mRNA expression level of CYP11B2, an aldosterone synthase, was very low, if it was present in the heart at all. It was reported that at normal plasma levels of adrenal steroids, more than 99% of nonepithelial mineralocorticoid receptors were occupied by glucocorticoids (Funder 2010). Under normal circumstances such occupancy is presumably in tonic inhibitory mode, but it enters active mode during tissue damage and generation of reactive oxygen species or under inappropriate sodium conditions (Funder 2010). Thus, it is possible that mineralocorticoid receptor signaling is activated in the heart of GC-A KO mice. The precise molecular mechanism by which GC-A signaling interacts with mineralocorticoid receptor signaling is still unclear.

Roles of the GC-A signaling in acute myocardial infarction

A number of experimental and clinical studies revealed that expression of ANP and especially BNP are increased in the infarct region of the ventricle. Plasma levels of ANP and BNP are also increased in the acute phase of acute myocardial infarction (AMI) in humans; plasma BNP increases especially rapidly, decreases within 24 h, increased again within 7 days, and then decreases gradually (Morita et al. 1993). When patients are treated with angiotensin-converting enzyme inhibitor, this second peak is obscured (Mizuno et al. 1997), suggesting that the second transient elevation of plasma BNP levels is related to healing processes after infarction. Thus, ANP and BNP have some pathological roles in AMI as hormones and (or) paracrine factors.

To investigate the roles of GC-A signaling in AMI, we generated permanent coronary occlusion models and ischemia–reperfusion models in GC-A KO mice and BNP transgenic (BNP-Tg) mice. When GC-A KO and wild-type mice were subjected to permanent coronary ligation, the GC-A KO mice exhibited lower survival rates and more severe ventricular fibrosis and postinfarct hypertrophy than wild-type mice (Nakanishi et al. 2005). GC-A KO mice with AMI died within 7 days after ligation; a major cause of death was probably heart failure, because lung weight is significantly heavier in GC-A KO mice. Urine volume and urinary excretion of sodium decreased just after the operation in both genotypes of mice; GC-A KO mice recovered more slowly than wild-type mice, which may be related to the more severe heart failure in GC-A KO mice. Because GC-A KO mice are hypertensive, we investigated whether hydralazine treatment rescues the poor survival rate and ventricular remodeling in GC-A KO mice; however, this treatment rescued neither poor survival nor ventricular remodeling. Given that the phenotype of GC-A KO is almost blocked by crossing with mice lacking the AT1 gene, we generated an AMI model in GC-A and AT1 double-KO mice. The results were very interesting. Although chronic ventricular remodeling such as hypertrophy and fibrosis disappeared almost completely in double-KO mice (Figs. 3B and 3C), the survival rate in double-KO mice was the same as that in GC-A KO mice (Fig. 3A) (Nakanishi et al. 2005). These findings suggest that chronic ventricular remodeling is AT1 dependent, but acute death is not AT1 dependent. Therapeutic application of ANP in the acute phase may have some beneficial effects in AMI that cannot be replaced by angiotensin receptor blockers or angiotensin-converting enzyme inhibitors.

To determine whether GC-A signaling contributes to the extension of infarction in the very acute phase of AMI, we developed a model involving 30-min coronary artery ligation followed by 48-h reperfusion. Unexpectedly, infarct size assessed by triphenyltetrazolium chloride staining was significantly smaller in GC-A KO mice than in WT mice. Histological examination revealed that neutrophils were less infiltrated into the infarct region, with lower expression levels of P-selectin in coronary artery endothelium in GC-A KO mice. P-selectin is involved in the infiltration of neutrophils and plays a key role in reperfusion injury in myocardium; consistent with this, reperfusion injury is less severe in GC-A KO mice. Moreover, we confirmed that endothelial expression of P-selectin is transcriptionally promoted by NF-κB activation in which GC-A signaling is involved (Izumi et al. 2001).

We also generated a permanent occlusion model in mice overexpressing the BNP gene under control of the serum amyloid protein A promoter, in which mice BNP is not overexpressed in the heart but in the liver, and BNP is constitutively secreted from the liver, resulting in high levels of circulating BNP of ~10 ng/mL. When AMI was generated in BNP-Tg mice, BNP-Tg mice more frequently died ~3–5 days after the occlusion because of ventricular free-wall rupture, with more massive infiltration of neutrophils in the infarct region than in wild-type mice. In BNP-Tg mice, a higher expression of metalloproteinase-9 (MMP-9) was observed in infiltrated neutrophils by immunostaining and overactivation of MMP-9 and was confirmed by gelatin zymography. This result suggests that activation of MMP-9 was related to the free-wall rupture. BNP-Tg mice were rescued by treating with doxycycline, an inhibitor of MMP-9 (Kawakami et al. 2004). Recently, Kitakaze et al. (2007) disclosed that infusion of a low dose of ANP ($0.025\ \mu g \cdot mg^{-1} \cdot min^{-1}$) in patients with AMI reduced infarct size estimated by serum creatine kinase levels and improved ejection fraction at 6–12 months. Chen et al. (2009) also reported that low-dose infusion of BNP ($0.006\ \mu g \cdot mg^{-1} \cdot min^{-1}$) decreased the plasma aldosterone concentration and improved left ventricular ejection fraction in patients with anterior AMI. In the case of low-dose infusion of ANP or BNP, plasma ANP or BNP levels would reach at most 1ng/mL during the infusion period. So, the therapy with low-dose ANP or BNP is possibly safe and effective as an adjunctive therapy in AMI, though precautions should be taken with using high-dose ANP or BNP.

Conclusion

A number of experiments with whole GC-A KO mice and conditional GC-A KO mice have proven that GC-A signaling plays a protective role in cardiac hypertrophy and fibrosis by inhibiting several pathways promoting cardiac hypertrophy and fibrosis, one of which is RGS4-mediated inhibition of the G_q signal. Other molecular mechanisms remain to be elucidated.

References

Chen, H.H., Martin, F.L., Gibbons, R.J., Schirger, J.A., Wright, R.S., Schears, R.M., et al. 2009. Low-dose nesirtide in human anterior myocardial infarction suppresses aldosterone and preserves ventricular function and structure: a proof of concept study. Heart, **95**(16): 1315–1319. doi:10.1136/hrt.2008.153916. PMID: 19447837.

Funder, J.W. 2010. Aldosterone and mineralocorticoid receptors in the cardiovascular system. Prog. Cardiovasc. Dis. **52**(5): 393–400. doi:10.1016/j.pcad.2009.12.003. PMID:20226957.

Holtwick, R., Gotthardt, M., Skryabin, B., Steinmetz, M., Potthast, R., Zetsche, B., et al. 2002. Smooth muscle-selective deletion of guanylyl cyclase-A prevents the acute but not chronic effects of ANP on blood pressure. Proc. Natl. Acad. Sci. U.S.A. **99**(10): 7142–7147. doi:10.1073/pnas.102650499. PMID:11997476.

Holtwick, R., van Eickels, M., Skryabin, B.V., Baba, H.A., Bubikat, A., Begrow, F., et al. 2003. Pressure-independent cardiac hypertrophy in mice with cardiomyocyte-restricted inactivation of the atrial natriuretic peptide receptor guanylyl cyclase-A. J. Clin. Invest. **111**(9): 1399–1407. PMID:12727932.

Izumi, T., Saito, Y., Kishimoto, I., Harada, M., Kuwahara, K., Hamanaka, I., et al. 2001. Blockade of the natriuretic peptide receptor guanylyl cyclase-A inhibits NF-κB activation and alleviates myocardial ischemia/reperfusion injury. J. Clin. Invest. **108**(2): 203–213. PMID:11457873.

John, S.W., Krege, J.H., Oliver, P.M., Hagaman, J.R., Hodgin, J.B., Pang, S.C., et al. 1995. Genetic decreases in atrial natriuretic peptide and salt-sensitive hypertension. Science (Washington, D. C.), **267**(5198): 679–681. doi:10.1126/science.7839143. PMID: 7839143.

Kawakami, R., Saito, Y., Kishimoto, I., Harada, M., Kuwahara, K., Takahashi, N., et al. 2004. Overexpression of brain natriuretic peptide facilitates neutrophil infiltration and cardiac matrix metalloproteinase-9 expression after acute myocardial infarction. Circulation, **110**(21): 3306–3312. doi:10.1161/01.CIR. 0000147829.78357.C5. PMID:15545516.

Kitakaze, M., Asakura, M., Kim, J., Shintani, Y., Asanuma, H., Hamasaki, T., et al. 2007. Human atrial natriuretic peptide and nicorandil as adjuncts to reperfusion treatment for acute myocardial infarction (J-WIND): two randomised trials. Lancet, **370**(9597): 1483–1493. doi:10.1016/S0140-6736(07)61634-1. PMID:17964349.

Li, Y., Kishimoto, I., Saito, Y., Harada, M., Kuwahara, K., Izumi, T., et al. 2002. Guanylyl cyclase-A inhibits angiotensin II type 1A receptor-mediated cardiac remodeling, an endogenous protective mechanism in the heart. Circulation, **106**(13): 1722–1728. doi:10. 1161/01.CIR.0000029923.57048.61. PMID:12270869.

Li, Y., Kishimoto, I., Saito, Y., Harada, M., Kuwahara, K., Izumi, T., et al. 2004. Androgen contributes to gender-related cardiac hypertrophy and fibrosis in mice lacking the gene encoding guanylyl cyclase-A. Endocrinology, **145**(2): 951–958. doi:10. 1210/en.2003-0816. PMID:14592959.

Li, Y., Saito, Y., Kuwahara, K., Rong, X., Kishimoto, I., Harada, M., et al. 2010. Vasodilator therapy with hydralazine induces angiotensin AT receptor-mediated cardiomyocyte growth in mice lacking guanylyl cyclase-A. Br. J. Pharmacol. **159**(5): 1133–1142. doi:10.1111/j.1476-5381.2009.00619.x. PMID:20136844.

Lopez, M.J., Wong, S.K., Kishimoto, I., Dubois, S., Mach, V., Friesen, J., et al. 1995. Salt-resistant hypertension in mice lacking the guanylyl cyclase-A receptor for atrial natriuretic peptide. Nature (Lond.), **378** (6552): 65–68. doi:10.1038/378065a0. PMID:7477288.

Mizuno, Y., Yasue, H., Oshima, S., Yoshimura, M., Ogawa, H., Morita, E., et al. 1997. Effects of angiotensin-converting enzyme inhibitor on plasma B-type natriuretic peptide levels in patients with acute myocardial infarction. J. Card. Fail. **3**(4): 287–293. doi:10.1016/S1071-9164(97)90028-2. PMID:9547443.

Morita, E., Yasue, H., Yoshimura, M., Ogawa, H., Jougasaki, M., Matsumura, T., et al. 1993. Increased plasma levels of brain natriuretic peptide in patients with acute myocardial infarction. Circulation, **88**(1): 82–91. PMID:8319360.

Nakanishi, M., Saito, Y., Kishimoto, I., Harada, M., Kuwahara, K., Takahashi, N., et al. 2005. Role of natriuretic peptide receptor guanylyl cyclase-A in myocardial infarction evaluated using genetically engineered mice. Hypertension, **46**(2): 441–447. doi:10.1161/01.HYP.0000173420.31354.ef. PMID:15998711.

Nakao, K., Ogawa, Y., Suga, S., and Imura, H. 1992. Molecular biology and biochemistry of the natriureteic peptide system II: Natriureteic peptide receptors. J. Hypertens. **10**(10): 1111–1114. doi:10.1097/00004872-199210000-00002. PMID:1334991.

Sabrane, K., Kruse, M.N., Fabritz, L., Zetsche, B., Mitko, D., Skryabin, B.V., et al. 2005. Vascular endothelium is critically involved in the hypotensive and hypovolemic actions of atrial natriuretic peptide. J. Clin. Invest. **115**(6): 1666–1674. doi:10. 1172/JCI23360. PMID:15931395.

Sabrane, K., Kruse, M.N., Gazinski, A., and Kuhn, M. 2009. Chronic endothelium-dependent regulation of arterial blood pressure by atrial natriuretic peptide: role of nitric oxide and endothelin-1. Endocrinology, **150**(5): 2382–2387. doi:10.1210/en.2008-1360. PMID:19179430.

Tamura, N., Ogawa, Y., Chusho, H., Nakamura, K., Nakao, K., Suda, M., et al. 2000. Cardiac fibrosis in mice lacking brain natriuretic peptide. Proc. Natl. Acad. Sci. U.S.A. **97**(8): 4239–4244. doi:10. 1073/pnas.070371497. PMID:10737768.

Tang, K.M., Wang, G.R., Lu, P., Karas, R.H., Aronovitz, M., Heximer, S.P., et al. 2003. Regulator of G-protein signaling-2 mediates vascular smooth muscle relaxation and blood pressure. Nat. Med. **9**(12): 1506–1512. doi:10.1038/nm958. PMID: 14608379.

Tokudome, T., Kishimoto, I., Horio, T., Arai, Y., Schwenke, D.O., Hino, J., et al. 2008. Regulator of G-protein signaling subtype 4 mediates antihypertrophic effect of locally secreted natriuretic peptides in the heart. Circulation, **117**(18): 2329–2339. doi:10. 1161/CIRCULATIONAHA.107.732990. PMID:18443239.

Zhang, Q., Saito, Y., Naya, N., Imagawa, K., Somekawa, S., Kawata, H., et al. 2008. The specific mineralocorticoid receptor blocker eplerenone attenuates left ventricular remodeling in mice lacking the gene encoding guanylyl cyclase-A. Hypertens. Res. **31**(6): 1251–1256. doi:10.1291/hypres.31.1251. PMID:18716375.

Mutation-Linked Defective Interdomain Interactions Within Ryanodine Receptor Cause Aberrant Ca^{2+} Release Leading to Catecholaminergic Polymorphic Ventricular Tachycardia

Takeshi Suetomi, MD; Masafumi Yano, MD, PhD; Hitoshi Uchinoumi, MD, PhD; Masakazu Fukuda, MD; Akihiro Hino, MD; Makoto Ono, MD, PhD; Xiaojuan Xu, MD, PhD; Hiroki Tateishi, MD, PhD; Shinichi Okuda, MD, PhD; Masahiro Doi, MD, PhD; Shigeki Kobayashi, MD, PhD; Yasuhiro Ikeda, MD, PhD; Takeshi Yamamoto, MD, PhD; Noriaki Ikemoto, PhD; Masunori Matsuzaki, MD, PhD

Background—The molecular mechanism by which catecholaminergic polymorphic ventricular tachycardia is induced by single amino acid mutations within the cardiac ryanodine receptor (RyR2) remains elusive. In the present study, we investigated mutation-induced conformational defects of RyR2 using a knockin mouse model expressing the human catecholaminergic polymorphic ventricular tachycardia–associated RyR2 mutant (S2246L; serine to leucine mutation at the residue 2246).

Methods and Results—All knockin mice we examined produced ventricular tachycardia after exercise on a treadmill. cAMP-dependent increase in the frequency of Ca^{2+} sparks was more pronounced in saponin-permeabilized knockin cardiomyocytes than in wild-type cardiomyocytes. Site-directed fluorescent labeling and quartz microbalance assays of the specific binding of DP2246 (a peptide corresponding to the 2232 to 2266 region: the 2246 domain) showed that DP2246 binds with the K201-binding sequence of RyR2 (1741 to 2270). Introduction of S2246L mutation into the DP2246 increased the affinity of peptide binding. Fluorescence quench assays of interdomain interactions within RyR2 showed that tight interaction of the 2246 domain/K201-binding domain is coupled with domain unzipping of the N-terminal (1 to 600)/central (2000 to 2500) domain pair in an allosteric manner. Dantrolene corrected the mutation-caused domain unzipping of the domain switch and stopped the exercise-induced ventricular tachycardia.

Conclusions—The catecholaminergic polymorphic ventricular tachycardia–linked mutation of RyR2, S2246L, causes an abnormally tight local subdomain-subdomain interaction within the central domain involving the mutation site, which induces defective interaction between the N-terminal and central domains. This results in an erroneous activation of Ca^{2+} channel in a diastolic state reflecting on the increased Ca^{2+} spark frequency, which then leads to lethal arrhythmia. **(*Circulation*. 2011;124:682-694.)**

Key Words: calcium ■ CPVT ■ ion channels ■ sarcoplasmic reticulum ■ ventricular tachycardia

Ryanodine receptor (RyR2), the Ca^{2+} release channel in the cardiac sarcoplasmic reticulum (SR), plays a key role in cardiac excitation-contraction coupling.[1] A considerable body of evidence shows that RyR2 function is defective in failing hearts, causing spontaneous Ca^{2+} leak.[2] The Ca^{2+} leak leads to contractile dysfunction by reducing the SR Ca^{2+} content and also induces delayed afterdepolarization, which ultimately leads to lethal arrhythmia.[2] More than 120 RyR2 mutations have been identified in patients with catecholaminergic polymorphic ventricular tachycardia (CPVT) or arrhythmogenic right ventricular cardiomyopathy type 2.[3] RyR2 mutations are not randomly distributed, but they cluster into 3 definable regions. These domains are designated as the N-terminal domain (amino acids 1 to 600), the central domain (amino acids 2000 to 2500), and the C-terminal channel-forming domain. Because a single point mutation in any of these domains has a severe impact on the channel function, these domains must play a key role in regulating the channel function of both RyR2 and RyR1.

Clinical Perspective on p 694

Chiefly on the basis of the conformational probe approach, Ikemoto and colleagues[4–6] proposed that the N-terminal

Received February 2, 2011; accepted June 6, 2011.

From the Department of Medicine and Clinical Science, Division of Cardiology, Yamaguchi University Graduate School of Medicine, Ube, Yamaguchi, Japan (T.S., M.Y., H.U., M.F., A.H., M.O., X.X., H.T., S.O., M.D., S.K., Y.I., T.Y., M.M.); Boston Biomedical Research Institute, Watertown, MA (N.I.); and Department of Neurology, Harvard Medical School, Boston, MA (N.I.).

Guest Editor for this article was Michael E. Cain, MD.

The online-only Data Supplement is available with this article at http://circ.ahajournals.org/lookup/suppl/doi:10.1161/CIRCULATIONAHA.111.023259/-/DC1.

Correspondence to Masafumi Yano, MD, PhD, Department of Medicine and Clinical Science, Division of Cardiology, Yamaguchi University Graduate School of Medicine, 1-1-1 Minamikogushi, Ube, Yamaguchi, 755-8505, Japan. E-mail yanoma@yamaguchi-u.ac.jp

Circulation **is available at http://circ.ahajournals.org** **DOI: 10.1161/CIRCULATIONAHA.111.023259**

domain and the central domain interact with each other to act as the implicit on/off switch that opens and closes the channel, and the interacting domain pair was designated as a "domain switch." Parallel assays of the conformational state of RyR2 and the functional state of Ca^{2+} channel have shown that zipping of the interacting domains closes the channel, and unzipping opens it. A mutation in either domain weakens the interdomain interaction and causes domain unzipping in an otherwise resting state, which results in an erroneous activation of the channel and diastolic Ca^{2+} leak.[4–6] Consistent with the domain switch hypothesis, single-particle analysis of the 3-dimensional structure of the RyR2 molecule revealed that the N-terminal and central domains (located in domains 5 and 6 of the so-called clamp region, respectively) are in close apposition to each other.[7,8]

We have shown previously that in failing hearts, defective interaction between the N-terminal domain and the central domain of RyR2 induces Ca^{2+} leak even under the conditions of reduced SR Ca^{2+} load, leading to contractile dysfunction.[9] In normal hearts, these domains interact with each other to produce a zipped configuration, which stabilizes the closed state of the Ca^{2+} channel. However, in the failing heart, this interaction becomes loose because of oxidative stress[10] or protein kinase A (PKA)–mediated hyperphosphorylation and dissociation of FKBP12.6.[9] Domain unzipping destabilizes the closed state of the channel, resulting in diastolic Ca^{2+} leak. We have also shown that correcting the unzipped configuration to the normal zipped state by treatment with either K201 (JTV519)[9,11] or dantrolene[12] restores normal channel gating in otherwise leaky RyR2 channels of failing hearts.

Moreover, we recently demonstrated, using a transgenic mouse model in which CPVT-type R2474S mutation is knocked in the central domain of RyR2, that this mutation caused aberrant unzipping of the domain switch regions, lowering the threshold of luminal [Ca^{2+}] for channel activation, sensitizing the channel to PKA-dependent phosphorylation, and led to CPVT.[13] Dantrolene treatment that corrects the defective interdomain interaction prevented aberrant Ca^{2+} release, thereby preventing delayed afterdepolarization and CPVT.[13,14] These findings indicate that the defective interdomain interaction between the N-terminal and central domains, caused by single point mutation, oxidative stress, and/or PKA hyperphosphorylation, destabilizes the channel, leading to lethal arrhythmia and heart failure.

In our previous study of canine RyR2, we found that the domain switch is conformationally coupled with the interaction of subdomains (the 2114 to 2149 region and the 2234 to 2750 region) within the central domain, playing an important role in the regulation of channel function: Their tight interaction (subdomain zipping) opens the Ca^{2+} channel, and their dissociation (subdomain unzipping) closes the channel.[11] We then demonstrated several important features of the interaction: (1) Diastolic SR Ca^{2+} leak of failing heart happens as a result of erroneous zipping of these subdomains and channel activation in an otherwise resting state; (2) specific binding of K201 to RyR2 takes place at the 2114 to 2149 region, indicating that this is the K201-binding domain; and (3) the binding of K201 to this domain interferes with its interaction with the 2234 to 2750 region, thereby correcting aberrant domain zipping and diastolic Ca^{2+} leak in the failing RyR2.[11]

The aforementioned findings suggest the hypothesis that the S2246L (serine to leucine mutation at residue 2246) CPVT mutation in the 2234 to 2750 region (which we call *2246 domain*) causes an abnormal zipping between the 2246 domain and the K201-binding domain. To test this hypothesis, we used S2246L knockin mice. We demonstrate here that the S2246L mutation introduced into the 2246 domain causes an abnormally tight interaction with its partner domain (the K201-binding domain). Importantly, this mutation-induced tight zipping of these domains is coupled in an allosteric manner with unzipping of the domain switch. This leads to several phenotypes such as hypersensitized channel gating to luminal [Ca^{2+}] and to increased diastolic Ca^{2+} leak, the phenotypes that are commonly observed in the transgenic mouse models carrying different knockin CPVT mutations,[15–17] including our previously investigated R2474S/+ knockin model.[13]

Methods

An expanded Methods section is available in the online-only Data Supplement.

Animals

This study conforms to the *Guide for the Care and Use of Laboratory Animals* published by the US National Institutes of Health (NIH publication No. 85-23, revised 1996). The care of the animals and the protocols used were in accord with guidelines laid down by the Animal Ethics Committee of Yamaguchi University School of Medicine.

Peptides Used and Peptide Synthesis

We used the 3 domain peptides (DP), as described previously[13]: (1) DPc10: DP2460-2495; 2460GFCPDHKAAMVLFLDRVYGIEVQDFLLHLLEVGFLP2495; (2) DP2246:DP2232-2266; 2232PAMRGSTPLDVAAASVMDNNELALALREPDLEKVV2266; and (3) DP2246mut:DP2232-2266mut (serine2246 is mutated to leucine); *2232PAMRGSTPLDVAAAL*VMDNNELALALREPDLEKVV2266.

Analysis of Local Ca^{2+} Release Events

The local Ca^{2+} release events were measured in saponin-permeabilized cardiomyocytes, as described previously.[13] To avoid possible side effect of Ca^{2+}/calmodulin-dependent protein kinase II (CaMKII) on cAMP-induced change in Ca^{2+} sparks, CaMKII inhibitor KN-93 (1 μmol/L) was added.

Statistical Analysis

Paired or unpaired *t* test was used for statistical comparison of the data between 2 different situations, and ANOVA with a post hoc Scheffé test was used for statistical comparison of concentration-dependent data. Data for each different condition were obtained in the same preparation of SR or isolated cells originating from 10 to 16 hearts or 1 heart, respectively. Statistical comparison of data for these preparations was then performed. Data are expressed as mean±SE. We accepted a P value <0.05 as statistically significant.

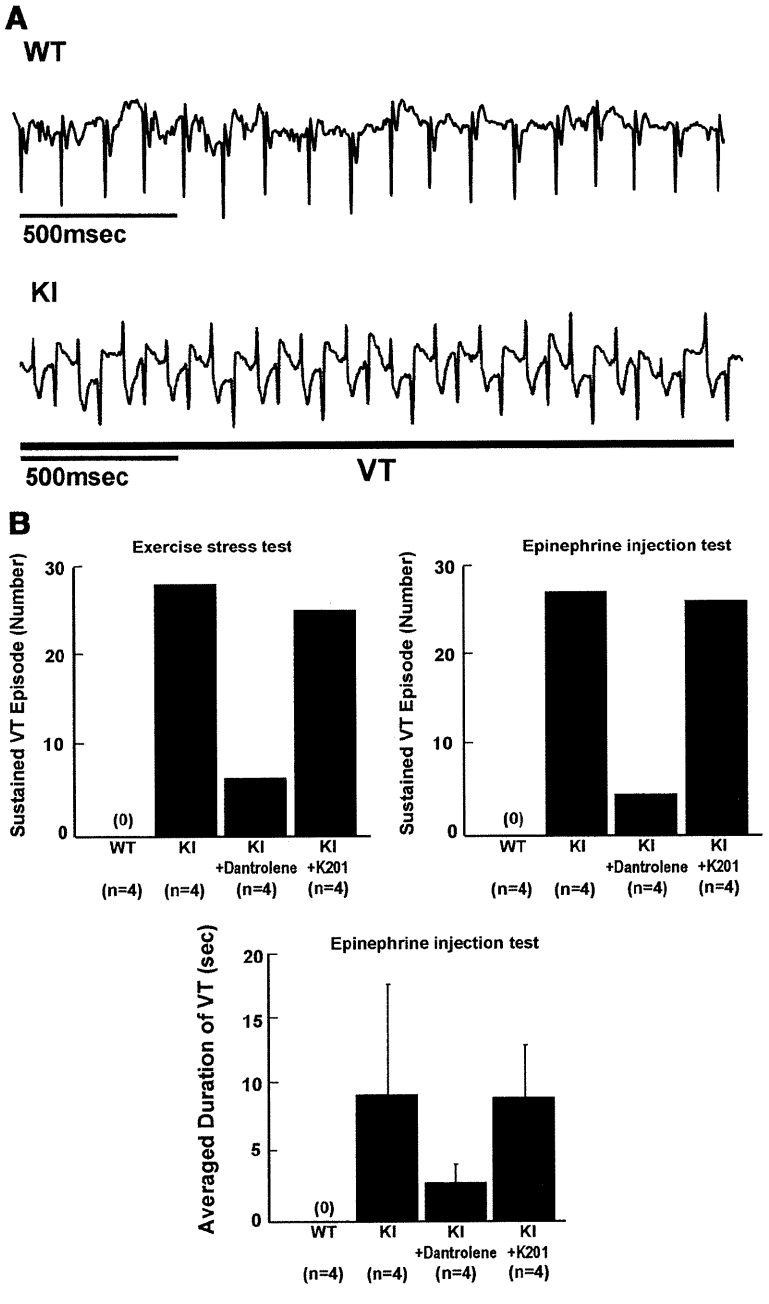

Figure 1. A, Representative ECG recordings in wild-type (WT) and knockin (KI) mice. In all KI mice examined, bidirectional or polymorphic ventricular tachycardia (VT) was induced by exercise on treadmill or epinephrine injection (2 mg/kg IP). **B**, Summarized data for the effect of dantrolene or K201 on exercise-induced or epinephrine-induced VT in KI mice. Data represent mean±SE of 4 hearts.

Results

No Appreciable Change in Structural and Functional Characteristics of S2246L/+ Knockin Mice at the Resting State

The hearts of wild-type (WT) and knockin mice showed no appreciable anatomic and histological abnormalities under baseline conditions (Figure IIA in the online-only Data Supplement) and no appreciable changes in the expression or phosphorylation levels of any of the SR proteins examined (Figure IIB in the online-only Data Supplement). Furthermore, echocardiography revealed no functional differences between WT mice and knockin mice (Figure III in the online-only Data Supplement).

Exercise or Epinephrine Induces Ventricular Tachycardia in S2246L/+ Knockin Mice, and Dantrolene Prevents Tachycardia

As shown in the ECG characteristics obtained from WT and knockin mice by telemetry (Table I in the online-only Data Supplement), there was no statistically significant difference in baseline parameters of heart rate, QT interval, and QTc between WT and knockin mice. Ventricular tachycardia (VT) was not observed in the resting condition (without stress) in WT or knockin mice. However, either treadmill exercise or epinephrine injection induced bidirectional or polymorphic VT in all knockin mice we examined but not in any of the WT mice tested (Figure 1A). In knockin mice, pretreatment with daily intraperitoneal injection of 20 mg/kg

dantrolene (7 to 10 days) prevented the VT (Figure 1B). Moreover, dantrolene significantly increased the total running distance during treadmill (treated: 178±55.3 m versus untreated: 59±10 m; $P<0.01$). On the other hand, pretreatment with K201 (JTV519) was without effect on the inducible VT (Figure 1B).

S2246L Mutation Reduces the Threshold of SR Ca^{2+} Load for Channel Activation

There was no appreciable difference in the level of PKA phosphorylation of RyR2 at Ser2808 between knockin and WT cardiomyocytes, both without and with added cAMP. The added cAMP was washed away to prevent further PKA phosphorylation (Figure 2A). The frequency of Ca^{2+} sparks increased with an increase of the concentration of cAMP (0.1 to 1 μmol/L) in both knockin and WT cardiomyocytes to a comparable degree (Figure 2B). However, because there was a considerable reduction in the SR Ca^{2+} content in knockin cardiomyocytes, the Ca^{2+} spark frequency per the releasable SR Ca^{2+} content was significantly higher in knockin cardiomyocytes than in WT cardiomyocytes. As a result, the plot of Ca^{2+} spark frequency versus SR Ca^{2+} content shows a considerable left shift compared with that of WT cardiomyocytes (Figure 2C). Even under the conditions in which the SR Ca^{2+} content was progressively reduced in the presence of thapsigargin (without cAMP), an inhibitor of SERCA2a, the SR Ca^{2+}-dependent increase of Ca^{2+} spark frequency was significantly higher in the knockin compared with the WT cardiomyocytes (Figure 2C); the increase of Ca^{2+} spark frequency was accompanied by the increase in both full width at half maximum and full duration at half maximum at matched SR Ca^{2+} content (Table II in the online-only Data Supplement). The effects of cAMP on Ca^{2+} spark characteristics of knockin cardiomyocytes are summarized in Table III in the online-only Data Supplement. In the knockin cardiomyocytes, the peak amplitude and full width at half maximum decreased, and the full duration at half maximum increased, suggesting a delay in RyR2 inactivation. Taken together, these data suggest that the thresholds of SR luminal [Ca^{2+}] for channel opening and for channel inactivation decreased considerably in the knockin cardiomyocytes because of the single S2246L mutation in RyR2.

PKA phosphorylation modulates not only RyR2 Ca^{2+} release but also SR Ca^{2+} uptake. Thus, we measured the Ca^{2+} spark frequency and SR Ca^{2+} content in the presence of 0.3 μmol/L thapsigargin (Figure 2D). Thapsigargin eliminated the cAMP-dependent Ca^{2+} spark frequency increase in both WT and knockin cardiomyocytes. This suggests that the cAMP-dependent Ca^{2+} spark frequency increase is primarily due to the activation of SR Ca^{2+} uptake and subsequent increase in SR Ca^{2+} load.

To determine whether preventing unzipping of the domain switch (see Introduction) reverses the leftward shift of the Ca^{2+} spark frequency/SR Ca^{2+} content dependence seen in the knockin cardiomyocytes, we used dantrolene, which was shown to bind to residues 602 to 620 of RyR2 and prevent both domain unzipping and abnormal Ca^{2+} release in failing hearts.[12] Dantrolene shifted the Ca^{2+} spark frequency/SR Ca^{2+} content plot to the right, resulting in a WT-like pattern (Figure 2E). However, K201, which prevented the development of heart failure,[18] did not correct the leftward shift of the Ca^{2+} spark frequency/SR Ca^{2+} content dependence in knockin mouse cardiomyocytes (Figure 2F; for the reason, see Discussion).

Probing the 2246 Domain/ K201-Binding Domain Interaction With DP2246 (a Domain Peptide Corresponding to the 2246 Domain)

To localize the partner domain to which DP2246 binds, we first labeled RyR2 using the peptide-mediated site-directed methylcoumarin acetamido (MCA) labeling technique.[6,9] Then the MCA-labeled RyR2 was subjected to tryptic digestion to analyze the degradation of the fluorescently labeled polypeptide chain by sodium dodecyl sulfate–polyacrylamide gel electrophoresis and immunomapping with site-specific antibodies. As shown in Figure 3A, DP2246-mediated photoaffinity labeling of the fluorescent probe MCA resulted in specific fluorescent labeling of RyR2. The presence of an excess concentration of unlabeled DP2246 (10 mmol/L) prevented DP2246-mediated MCA labeling. Ab2141 (an antibody raised against the K201-binding domain), but not nonimmune IgG, prevented DP2246-mediated MCA labeling. These results indicate that DP2246 binds specifically to the K201-binding domain.

The MCA-labeled RyR2 polypeptide chain was degraded to 210-, 155-, 125-, and then to 60-kDa fragments, all of which were immunostained with Ab2141, an antibody directed against the central region (Figure 3B). Furthermore, of several recombinant RyR2 fragments, which span residues 1 to 2750, only the fragment 1741 to 2270 was specifically labeled with MCA (Figure 3C). These data suggest that DP2246 interacts with the 1741 to 2270 region of RyR2, which includes the previously reported 2114 to 2149 K201-binding domain.[11]

To further verify the DP2246-binding domain of RyR2, we used the quartz crystal microbalance binding assay as an in vitro model of domain-domain interaction. As shown in Figure 4A, DP2246 rapidly bound to fragment 1741 to 2270 but not to other recombinant fragments. Ab2141, but not nonimmune IgG, abolished DP2246 binding to fragment 1741 to 2270 (Figure 4B). This further supports the notion that DP2246 binds to the K201-binding domain (residue 2114 to 2149) within the 1741 to 2270 residue region.

S2246L Mutation Increases the Affinity of Binding of DP2246 to RyR2

As the first approach to test the hypothesis that the S2246L CPVT mutation in the 2246 domain causes an abnormal zipping between the 2246 domain and the K201-binding domain (see Introduction), we performed the binding assay of DP2246 and DP2246mut (DP2246, in which S2246L mutation is introduced) to RyR2 using the peptide-mediated site-directed MCA labeling technique.[6,9] The fluorescence labeling mediated by DP2246mut is also site-specific to the K201-binding domain, as indicated by both cold-chase and antibody-chase experiments, but, importantly, the intensity of

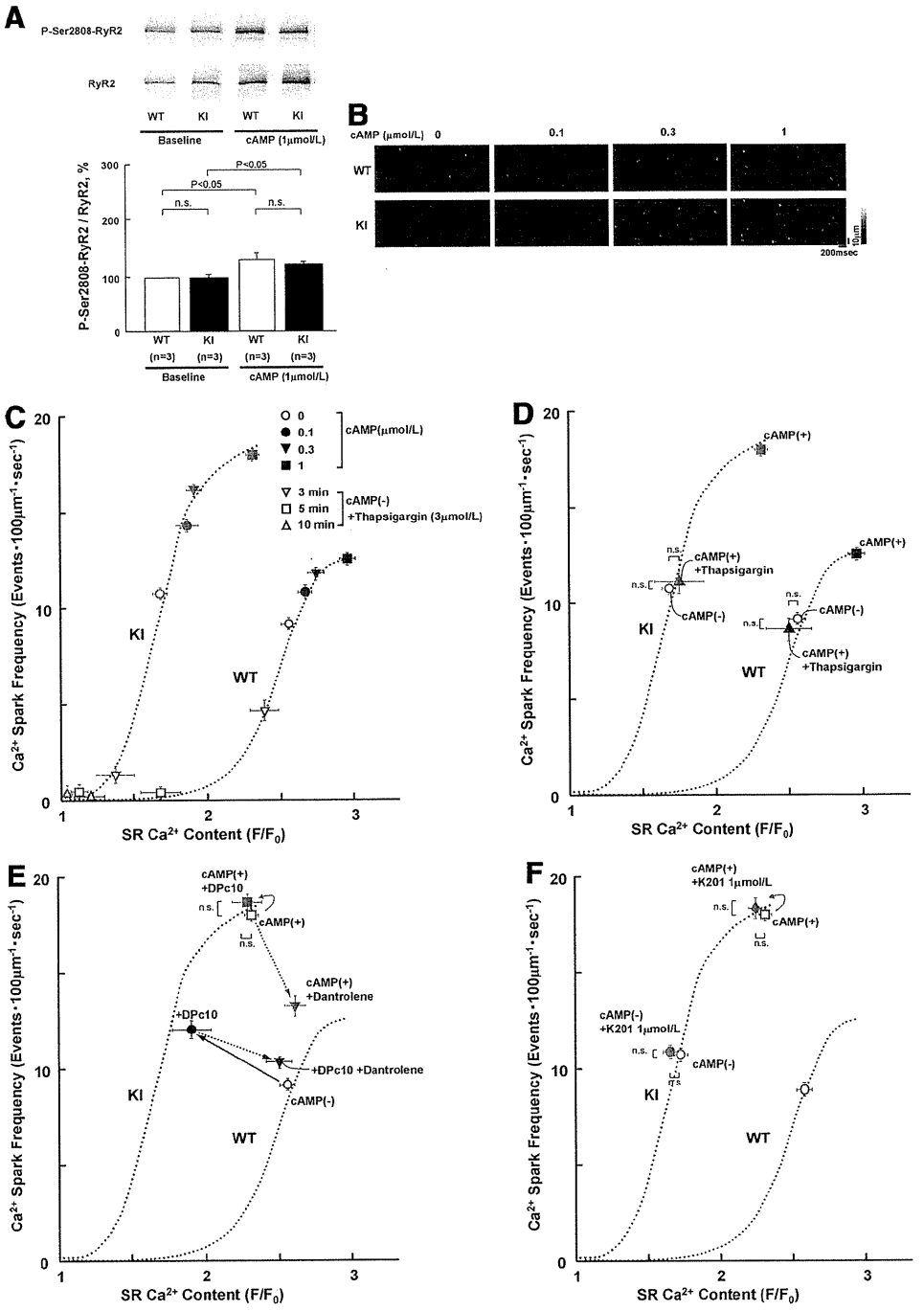

Figure 2. Protein kinase A phosphorylation at Ser2808 in ryanodine receptor (RyR2) (P-Ser2808-RyR2) and local Ca^{2+} release events in saponin-permeabilized cardiomyocytes. **A**, Comparison of P-Ser2808-RyR2 in knockin (KI) and wild-type (WT) cardiomyocytes. In the presence of cAMP (1 μmol/L), okadaic acid (1 μmol/L), and CaMKII inhibitor KN-93 (1 μmol/L), KI and WT cardiomyocytes were incubated in the lysis buffer and centrifuged. Then the supernatant fraction containing crude homogenate was used for phosphorylation assay. N indicates the number of cell lysates from 3 to 4 hearts. **B**, Representative line-scan images of cardiomyocytes after addition of cAMP (0.1 to 1 μmol/L), at 30 nmol/L [Ca^{2+}] buffered by 0.5 mmol/L EGTA. **C**, The plots of Ca^{2+} spark frequency vs sarcoplasmic reticulum (SR) Ca^{2+} content. SR Ca^{2+} content was measured by addition of 10 mmol/L caffeine. To obtain the data at lower SR Ca^{2+} contents, thapsigargin was added to the cardiomyocytes. Then both Ca^{2+} sparks and SR Ca^{2+} content were measured at 3, 5, and 10 minutes after the addition of thapsigargin (WT: n=4 to 5 hearts; KI: n=4 to 5 hearts). **D**, Effect of protein kinase A phosphorylation on Ca^{2+} spark frequency during inhibition of SR Ca^{2+} uptake in WT and S2246L/+ KI saponin-permeabilized cardiomyocytes. For protein kinase A phosphorylation of RyR2, both cAMP (1 μmol/L) and okadaic acid (1 μmol/L) were added to the cardiomyocytes at 30 nmol/L [Ca^{2+}] buffered by 0.5 mmol/L EGTA. Two minutes after the addition of cAMP, the added cAMP was washed away to prevent further protein kinase A phosphorylation. Then thapsigargin (0.3 μmol/L) was added. One minute later, line-scanned images were obtained (WT: n=4 to 5 hearts; KI: n=4 to 5 hearts). **E**, The dependence of Ca^{2+} spark frequency on SR Ca^{2+} content in the absence or in the presence of DPc10 or dantrolene. Arrow indicates the shift of the data points in the absence or in the presence of DPc10 (50 μmol/L) or dantrolene (1 μmol/L) (WT: n=4 to 5 hearts; KI: n=4 to 5 hearts). **F**, The dependence of Ca^{2+} spark frequency on SR Ca^{2+} content in the absence or in the presence of K201 (1 μmol/L) (WT: n=4 to 5 hearts; KI: n=4 to 5 hearts).

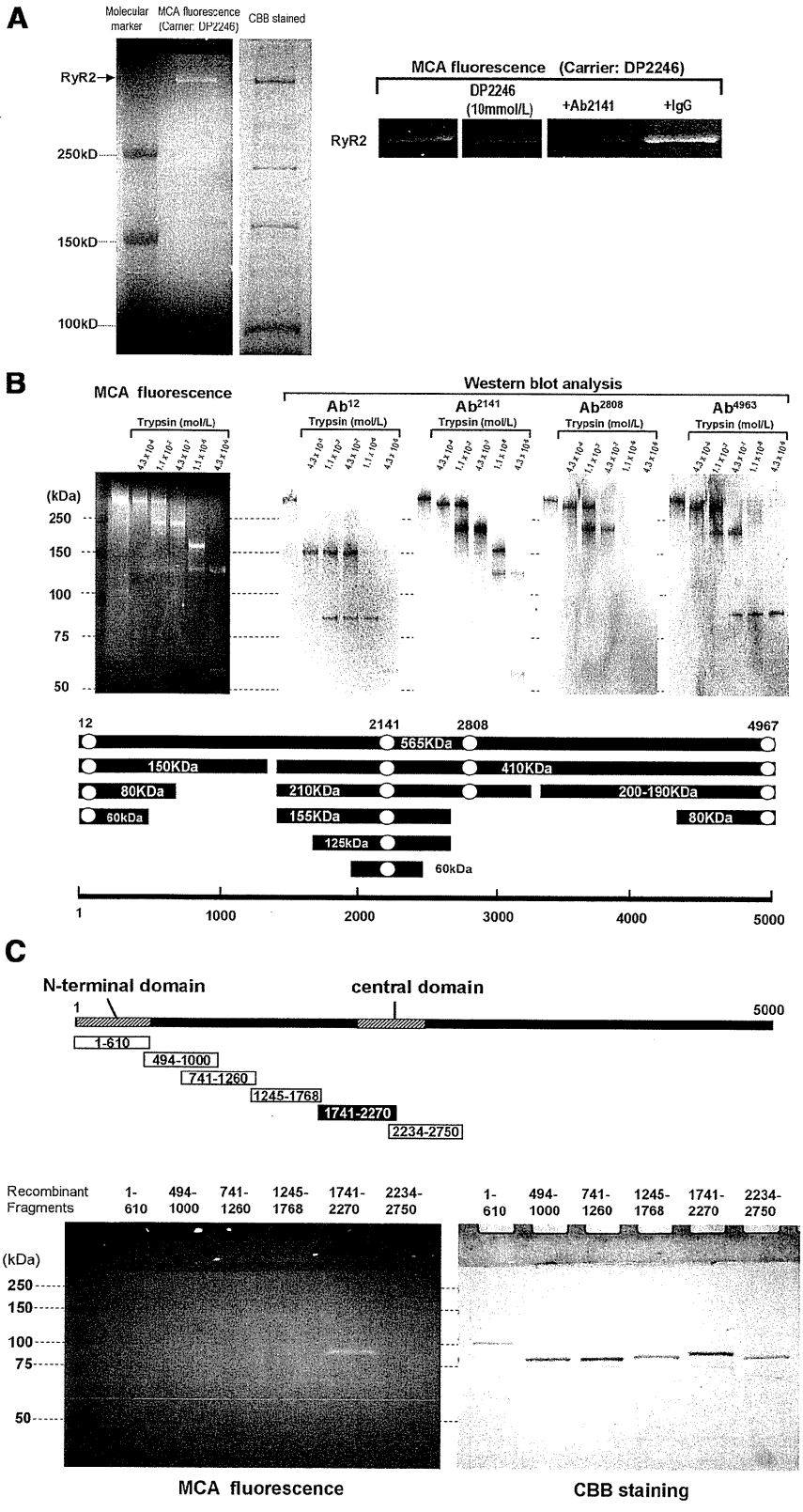

Figure 3. A, Site-directed fluorescence labeling of the ryanodine receptor (RyR2) with methylcoumarin acetamido (MCA). MCA fluorescence labeling took place specifically on RyR2 (fluorescence image, top left) of many sarcoplasmic reticulum proteins (Coomassie Brilliant Blue [CBB] protein staining, top right), with DP2246 used as the carrier. MCA fluorescence was barely detected when either an excess concentration of DP2246 (10 mmol/L) (cold chase) or Ab2141 (antibody against the K201-binding domain) was added during the labeling, indicating that DP2246-mediated fluorescent labeling was site specific. Three exogenous proteins with molecular weight (in kDa) 250, 150, and 100 were used as molecular markers. **B**, Identification of the partner domain of DP2246 in the tryptic fragments of the fluorescence-labeled RyR2. With the use of DP2246 as the site-directed carrier, MCA fluorescence labeling took place within RyR2 in SR vesicles. After tryptic digestion of the fluorescently labeled RyR2, the 60-kDa fragment was detected as the shortest MCA-labeled segment of the RyR2 by Ab2141. Ab2141 indicates antibody against K201-binding domain (epitope ^{2134}MGKEEEKLMIRGLGDI^{2149}); Ab12, antibody against N-terminal region (epitope ^{6}EGEDEIQFLRTDDE^{19}); Ab2808, antibody against phosphorylation site (epitope ^{2801}YNRTRRISQT^{2810}); and Ab4963, antibody against C-terminal region (epitope ^{4959}RKQYEDQLN^{4967}). **C**, Identification of the partner domain of DP2246 by site-specific MCA labeling of recombinant RyR2 fragments. Of several recombinant RyR2 fragments (1 to 610, 741 to 1260, 1245 to 1768, 1741 to 2270, 2234 to 2750), only the fragment1741 to 2270 was specifically MCA labeled.

the MCA label of RyR2 is significantly higher than that of the DP2246-mediated labeling (Figure 5A).

To assess the affinity of binding of DP2246 to its partner domain, we plotted the extent of peptide-mediated site-directed MCA fluorescence labeling of RyR2 as a function of the concentration of DP2246 or DP2246mut (Figure 5B). The apparent K_d of peptide binding to the K201-binding domain was 0.09 μmol/L with DP2246mut and 0.3 μmol/L with DP2246, indicating that the S2246L mutation in the 2246 domain produced a significant enhancement of the

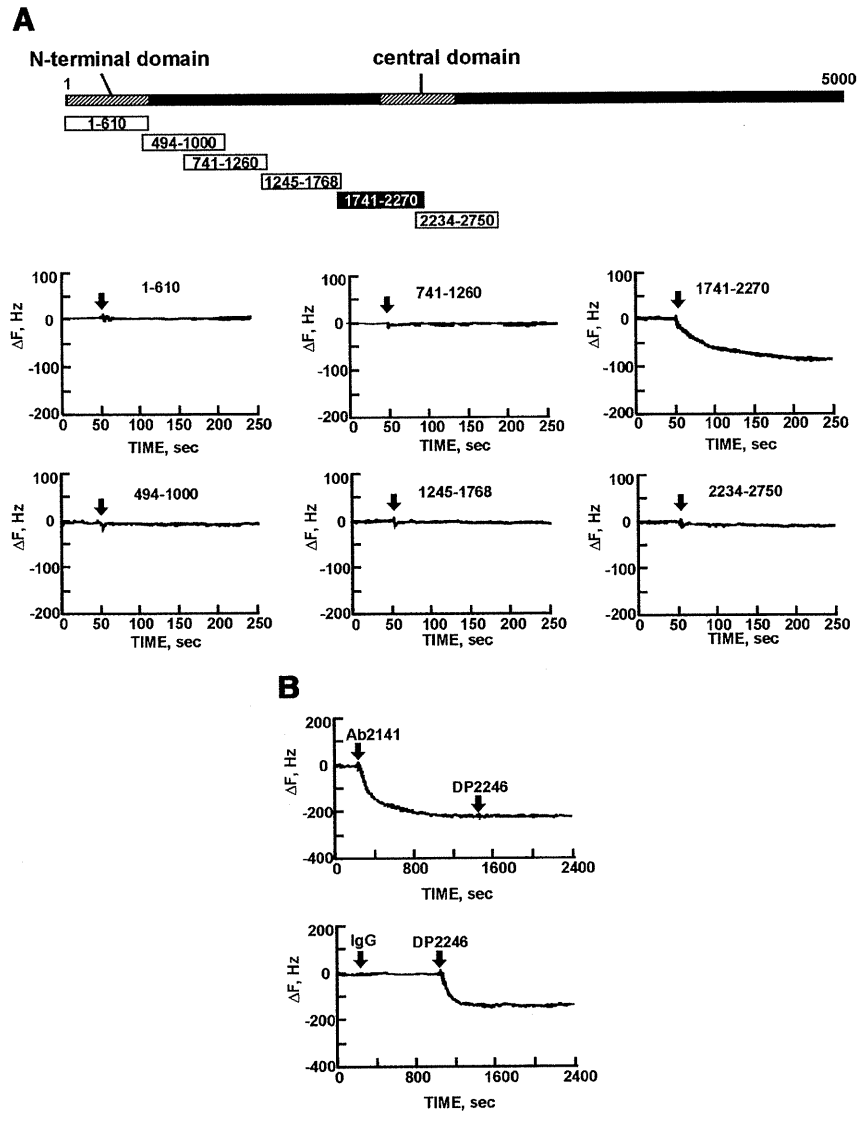

Figure 4. Screening of the binding partner of DP2246 with the use of quartz crystal microbalance binding assays of recombinant ryanodine receptor (RyR2) fragments. **A**, Time course of the binding of DP2246 to various RyR2 fragments. DP2246 was immobilized on the sensor chip surface as described in Expanded Materials and Methods in the online-only Data Supplement. **B**, Time course of the binding of DP2246 to the fragment 1741 to 2270 in the presence of Ab2141, an antibody against the K201-binding site, or nonimmune IgG.

interaction of DP2246 with its target domain (ie, K201-binding domain).

In Vivo DP2246 Binding in Wild-Type and Knockin Cardiomyocytes

To assess the peptide binding to RyR2 in in vivo conditions, we fluorescently labeled DP2246 or DP2246mut with Oregon Green and introduced them into saponin-permeabilized cardiomyocytes. In WT cardiomyocytes, both the DP2246 binding signal and the DP2246mut binding signal were detected as green bands localized along the sarcomeres (Figure 6). As shown in the middle panel of Figure 6, DP2246mut showed higher binding affinity than DP2246 in the WT cardiomyocytes. In contrast, the fluorescence signal of both DP2246 and DP2246mut was barely detectable in the knockin cardiomyocytes. The plot of the intensity of the fluorescence along the sarcomeres (see Methods) as a function of the concentration of DP2246 (or DP2246mut) (Figure 6; bottom) shows that in the WT cardiomyocytes, maximal binding of both peptides takes place at 3 μmol/L peptides (K_d with DP2246mut probe, 0.08 μmol/L; K_d with DP2246 probe, 0.14 μmol/L). In the knockin cardiomyocytes, however, the binding is very partial even at the maximal concentration of the peptide we tested (3 μmol/L). This suggests that the S2246L mutation leads to an abnormally strong interaction between the 2246 domain and the K201 domain, which precludes the binding of DP2246 and DP2246mut to the K201 domain of knockin RyR2.

Mutation-Induced Aberrant Tight Interaction of the 2246 Domain/K201-Binding Domain in S2246L/+ Knockin Cardiomyocytes Causes Aberrant Unzipping of the Domain Switch

To investigate whether the domain switch is defective in S2246L/+ knockin mice, we adopted the fluorescence quench technique,[6,9] which permits us to spectroscopically monitor whether the domains are zipped or unzipped.

As in our previous study,[13] the N-terminal domain of RyR2 was labeled with the fluorescent probe MCA with the use of DPc10 as a site-directing carrier (see Figure in the online-

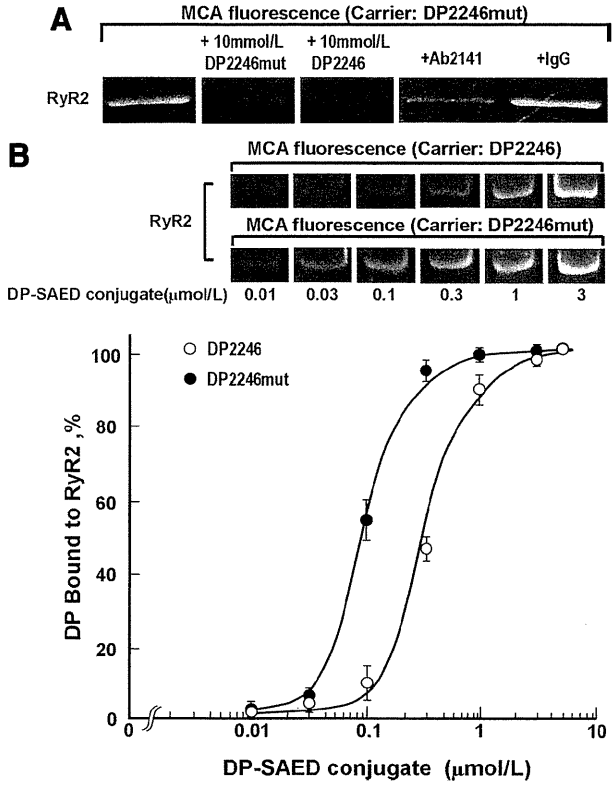

Figure 5. A, Site-directed fluorescence labeling of the ryanodine receptor (RyR2) with methylcoumarin acetamido (MCA) by using DP2246mut as the carrier. MCA fluorescence was barely detected when either an excess concentration of DP2246/2246mut (10 mmol/L) (cold chase) or Ab2141 (antibody against the K201-binding domain) was added during the labeling. **B,** Concentration dependence of DP2246 or DP2246mut on the binding to the RyR2. Data are mean±SE of 3 experiments with 3 SR preparations from 30 hearts. DP indicates domain peptide. SAED indicates sulfosuccinimidyl 3-((2-(7-azido-4-methylcoumarin-3-acetamido) ethyl) dithio) propionate.

only Data Supplement of Reference 11). As shown previously, in a zipped configuration of the domain switch, the attached MCA probe is inaccessible to a large fluorescence quencher QSY–bovine serum albumin conjugate; in an unzipped configuration, because of an opened gap between the interacting domains, the quencher becomes accessible to the attached MCA probe to quench the MCA fluorescence. In agreement with our previous study,[13] the extent of fluorescence quenching (K_Q: the Stern-Volmer quenching constant determined from the slope of the plot, which is a measure of the extent of domain unzipping) of the MCA increased when the WT SR was treated with domain unzipping peptide DPc10 (Figure 7A). In the knockin (S2246L/+) SR, on the other hand, the K_Q showed a high value even before the addition of DPc10, which was comparable to the level that was reached by addition of DPc10 to the WT SR; the addition of DPc10 to the knockin SR produced no further increase in the K_Q value (Figure 7B). These results suggest that S2246L mutation in the 2246 domain produced an allosteric effect on the domain switch, making it unzip, which is the same net result as would have been produced by the domain switch mutation R2474S.

Addition of dantrolene or K201 to the WT SR reduced the K_Q, indicating that the defective, or unzipped, configuration of the domain switch that had been produced by DPc10 treatment was restored to a normal zipped configuration (Figure 7A). Addition of dantrolene to the knockin SR also reduced the K_Q, indicative of recovered normal zipped configuration (Figure 7B). However, K201 was without effect on knockin SR (Figure 7B), presumably owing to the fact that the interaction between the 2246 domain and the K201-binding domain was so tight that K201 was inaccessible to the drug-binding domain.

The in vitro and in vivo assays of DP2246 binding to RyR2 (Figures 5 and 6) and the fluorescence quench assay of the domain switch (Figure 7B) suggest that the S2246L mutation causes aberrant zipping between the 2 subdomains within the central domain (namely, the 2246 domain and the K201-binding domain), and this produced unzipping of the domain switch in an allosterically coupled manner. To test this postulated conformational coupling between the 2 regions (namely, domain zipping of the 2246 domain/K201-binding domain pair and reciprocally coupled domain unzipping of the domain switch), we performed site-specific MCA labeling of the K201 domain of the WT RyR2. We then performed the fluorescence quench assay using QSY–bovine serum albumin, following the same principle as described above. As shown in Figure 7A (right), unzipping of the domain switch by DPc10 produced zipping of the 2246 domain/K201 domain pair, as evidenced by a significant reduction in the K_Q. Addition of dantrolene (50 μmol/L), which completely restored the normal zipped state of the domain switch (Figure 7A; left), produced no appreciable effect on the 2246 domain/K201-binding domain interaction (Figure 7A; right). However, K201 (1 μmol/L) completely restored the normal unzipped state of the 2246 domain/K201-binding domain pair from the DPc10-induced zipped state (Figure 7A; right).

In the knockin RyR2, DP2246 was virtually inaccessible to the K201-binding domain because of tight interaction of the in vivo 2246 domain with the K201-binding domain, as described above. For this reason, we could not perform site-specific fluorescent labeling for the fluorescence quench assay of the 2246 domain/K201-binding domain interaction. However, in light of the data shown in Figure 7B, we assume that the addition of DPc10 to the knockin RyR2 would produce no further change because unzipping of the domain switch and the coupled zipping of the 2246 domain/K201-binding domain pair would have already taken place.

FKBP12.6 Binding to the RyR2 Remains Unaltered in Knockin RyR2 Mice

According to several reports,[19,20] dissociation of RyR2-bound FKBP12.6 and resultant channel destabilization may be involved in both heart failure and lethal arrhythmia. We examined whether the CPVT mutation produced any effect on the RyR2-bound FKBP12.6 using a pull-down assay. As shown in Figure IV in the online-only Data Supplement, there